Light Scattering from Dilute Poly(styrene) Solutions in Uniaxial Elongational Flow

Malika J. Menasveta and David A. Hoagland*

Department of Polymer Science and Engineering, University of Massachusetts, Amherst, Massachusetts 01003

Received November 9, 1990; Revised Manuscript Received January 17, 1991

ABSTRACT: An angular-dependent light-scattering apparatus has been constructed to measure the deformation of dilute polymer chains dissolved in a solvent undergoing steady uniaxial elongational flow. The scattering measurements correspond to a small fluid volume, $\sim(50\ \mu m)^3$, centered at the stagnation point of an opposed jets flow device capable of strain rates up to 20 000 s^{-1}. We discuss here the deformation of 20×10^6 MW poly(styrene) dissolved in toluene at room temperature. Analysis of angular-dependent intensity by the Zimm plot method reveals a maximum molecular extension ratio ($R_{g,\parallel}/R_{g,eq}$) of order 2, attained at elongation rates significantly exceeding the inverse of the chain relaxation time τ. To transform intensity information to size measurements, corrections for the optical anisotropy of the flowing solution must be applied; these corrections reflect apparent coupled solvent/segment orientation.

Introduction

The striking elongational rheology of a dilute polymer solution reflects the complex dynamics associated with stretching and orientation of an isolated polymer chain surrounded by solvent. In the presence of a "strong" flow field—one possessing high strain rates and little vorticity—the characteristic random coil conformation of a flexible, linear molecule is significantly altered. At the same time, the elongational viscosity of its solution rises dramatically, by 1 order of magnitude or more. This phenomenon has aroused considerable industrial interest, for it plays a major role in processes such as spinning of low-concentration polymer solutions to form fibers, turbulent drag reduction, and rheology modification in enhanced oil recovery fluids. It has often been postulated that sufficiently large elongational stresses will result in the unraveling of the polymer coil to its fully extended conformation;[1,2] no definitive proof of complete unraveling, however, has yet been offered.

Theories for polymer deformation in flow have been intensely investigated,[3-15] using models from the basic dumbell to the more complicated bead–spring models of Rouse[16] and Zimm[17] or the freely jointed bead–rod model proposed by Kramers.[18] Recent enhancements include nonpreaveraged hydrodynamic interactions[10,11] and time-resolved computer simulation of the chain conformation in transient flow.[12,15] Each model predicts a longest chain relaxation time τ that must be multiplied by the strain rate $\dot{\epsilon}$ to ascertain the ability of a particular flow to deform the chain. For steady elongational flows this product is referred to as the Deborah number De. Summarizing many studies, flexible polymers are predicted to adopt a highly elongated conformation when the De exceeds a critical value of order 1; in most models, in fact, it is assumed a priori that the chain is fully unraveled. At low De, on the other hand, only limited stretching of the chain occurs, and predictions of the stretching level as a function of De vary between the different models. Whether the elongated, high De conformation persists when the De is lowered below its critical value remains controversial. Not addressed in current models is the presence or absence, in real systems, of large conformational barriers that could "trap" stretched conformations for times greater than τ. Such barriers could arise from intramolecular entanglements or the mutual uncrossability of polymer chains; these are important issues, inasmuch as the residence time in high-De regions remains finite in all real systems.

Experimentalists have principally focused on birefringence[1,2,19-27] and rheology[19,27] to determine *indirectly* the extent of polymer deformation in uniaxial and planar elongational flows. Birefringence, sensitive only to average segmental orientation, reveals no direct information about the global chain conformation. Only by hypothesizing a relationship between segmental orientation and chain conformation can this method be used to infer the global response to elongational flow. In addition, difficulty arises when birefringence data are interpreted since the optical anisotropy of a statistical segment may depend strongly on the choice of solvent.[28,29] Rheological experiments reveal information at length scales comparable to the chain's end-to-end distance. These experiments, unfortunately, require homogeneous deformation of macroscopic volumes of material, a constraint nearly impossible to satisfy when studying "strong" elongational flows of low-viscosity fluids.

Scattering is perhaps the only direct method for studying the global and local conformations of polymer chains in solution. When the appropriate wavelength is employed, flow-induced deformation of high molecular weight polymers in dilute solution can be measured unambiguously. The application of light scattering to flow environments has been rare, probably due to experimental difficulties encountered in conducting a light-scattering experiment in a homogeneous flow field. Only two previous investigations have employed light scattering to study the deformation of flexible polymers in elongational flow.[30,31] Smith et al.[30] probed the conformational changes of high molecular weight polymers in a flow-through orifice geometry. They reported that the maximum stretching ratio was $\sim$4, much less than expected for an affine deformation at the high De and contraction ratio of their flow. Lumley[31] employed a similar flow geometry and reached essentially the same conclusions. Intramolecular entanglements were subsequently postulated to play an important role in constraining the extent and/or rate of chain deformation.[32] In addition, chain deformation in transient elongational flows, such as those investigated by Smith et al. and Lumley, is likely to be smaller than in steady flow.

We have developed a light-scattering apparatus capable of measuring the deformations of dilute polymer chains in nearly homogeneous, steady uniaxial elongational flow.

0024-9297/91/2224-3427$02.50/0

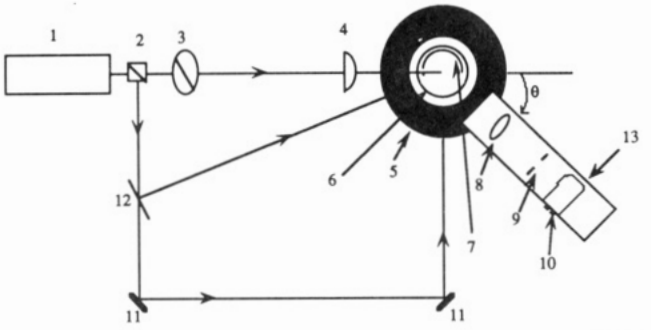

Figure 1. Components of the light scattering apparatus. Key: (1) 10-mW HeNe laser, (2) beam splitter, (3) vertical polarizer, (4) condenser lens, (5) rotary table, (6) glass vat, (7) anodized semicircular aluminum sleeve, (8) objective lens, (9) vertical slit, (10) photomultiplier tube, (11) mirrors, (12) mirror-type beam splitter, (13) aluminum arm, on which the detector optics are mounted.

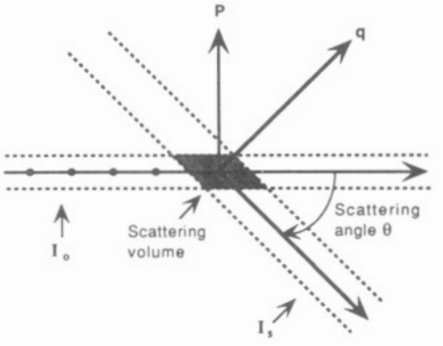

Figure 2. The scattering geometry indicating the relative orientations of the incident light vector $\mathbf{I}_o$, the scattered beam $\mathbf{I}_s$, the scattering vector $\mathbf{q}$, and the principal axis of stretching $\mathbf{P}$.

The flow is generated by withdrawing fluid through two cylindrical opposed jets, a geometry pioneered by Keller and Odell;[1] this arrangement permits studies across the full range of De. Light scattered from a small volume located at the stagnation point is measured as a function of scattering angle. We present here preliminary results for this scattering—and the corresponding levels of chain stretching—in dilute solutions of a 20×10^6 MW poly(styrene). In future contributions the dependence of the chain stretching on variables such as molecular weight, solvent viscosity, and solvent quality will be discussed in more detail.

Experimental Section

Light-Scattering Apparatus. The scattering apparatus, illustrated in Figure 1, combines features of conventional static and dynamic light-scattering instruments. The entire setup is mounted on a large vibration-free table (Newport). Collimated light emitted from the intensity-stabilized, vertically polarized 10-mW HeNe source laser is initially divided by a nonpolarizing beam-splitting cube into a parallel incident beam and a perpendicular alignment beam. The incident beam passes through a Glan-Thompson prism polarizer (Karl Lambert) and a condenser lens (f = 250 mm), which focuses the vertically polarized 632.8-nm light to a beam waist of approximately 140 μm[33] at the center of the scattering vat. The vat is a polished, 10.16 cm diameter precision glass cylinder (Wilmad Glass) with 0.68 cm thick walls; it holds up to 500 mL of polymer solution. To block extraneous light emanating from the point of beam impingement on the glass, a 600-μm pinhole is positioned inside the vat, directly against its inner wall. This anodized pinhole remains immersed in the polymer solution during the scattering experiment. A removable light trap (neutral density filter, D = 4.0) is placed against the vat's far side, angled downward to absorb and reflect the exiting beam out of the scattering plane. The glass vat is securely sealed inside the rim of a Teflon plate. This plate, in turn, is fitted inside an anodized aluminum jacket possessing a machined, semicircular strip window at the appropriate height for the detection optics. Horizontal set screws in the jacket allow the in-plane location of the vat to be controlled with high precision, while set screws through the base of the Teflon plate permit accurate vertical alignment.

The aluminum jacket is mounted to the optical table through a 7.5 cm diameter hole located at the center of a 30.0 cm diameter rotation stage (New England Affiliated Technologies). Bolted to this stage is a rigid, 1-m optical rail on which the detection optics, consisting of an objective lense ($f1$ = 60 mm, $f2$ = 80 mm), a 150 μm wide vertical slit, and a photomultiplier (Hamamatsu, Model R928) with housing (Products for Research, Model PR-1405RF), are attached. The objective lens collimates the scattered light such that an image, corresponding to ~100-μm region in the vicinity of the stagnation point, is formed at the plane of the slit. A computer-controlled stepper motor regulates the angular position of the optical rail over the experimentally accessible range of 0–120°, with a lead brick forming a counterweight during the rotation. The angular acceptance of the detection optics is less than 0.1°, and nominal wobble in the rotation stage is below 20″.

The scattered intensity is measured by photon counting (MIT, Models F-100E and PRM-100). In the worst case considered, the averaged dark pulse rate (600 counts/s) accounts for 10% of the solvent scattering (toluene, 90°). The linear dependence of the count rate on intensity, constrained by the detector's dead time, allows photon counting at rates up to 1.5×10^6 counts/s. Photon counting is automatically repeated 100 times for each angle, with the sampling time set to either 0.25 or 0.5 s. Anomalous scattering due to dust particles, especially at low angles, can be diminished by this rapid data sampling method. Intensity data are transferred to an IBM PC, where they are stored and analyzed according to a discrimination procedure developed by Haller et al.[34] The corrected data are then used to construct a Zimm plot from which the molecular weight, the radius of the gyration, and the second virial coefficient are obtained.

Meticulous adjustments are required to accurately position both the scattering volume and the flow device's stagnation point at the center of rotation of the detection optics. The perpendicular alignment beam (produced, as already described, by a beam-splitting cube) is divided into two additional beams; one is employed to ensure precise vertical alignment of the scattering vat and the second, which crosses the incident beam at the center of rotation, is used to ensure correct placement of the flow device. As an indication for correct alignment of the vat, the angular independence of the Rayleigh ratio of highly purified toluene is measured before each experiment. The scattered intensity $I(\theta)$ sin θ, corrected for the angular dependence of the scattering volume, remains constant (to within 0.5%) down to 17°, where appreciable stray light is first detected. The lowest angle employed for scattering is therefore 20°. Time-consuming efforts to further lower the angular range proved fruitless.

Insertion of crossed polarizers in the incident and detection optics, together with high-density optical filters to reduce incident intensity, makes possible measurement of relative flow birefringence (retardance). When such measurements are planned, the detection optics are rotated to 0°, and the transmitted light intensity is obtained by photon counting. Flow birefringence measurements permit precise vertical positioning of the jets, ensuring that the incident beam passes through the stagnation point. The remaining alignment beam then permits positioning of the stagnation point at the proper position along the incident beam to superpose this point with the center of the scattering volume.

A separate birefringence setup, consisting of a white light source (fiber optics illuminator, Dolan-Jennen Industries), a film analyzer and polarizer (Rolyn optics), and a microscope tube (Ealing Electro-optics) fitted with the appropriate objective lens, is used for visual birefringence observations. The main purpose of this setup is to assure collinearity and spacing of the jets, as well as to confirm that a stable birefringent line is present as ϵ increases.

Data Interpretation. Figure 2 outlines the scattering geometry, emphasizing the relative orientations of the incident

light vector $\mathbf{I}_0$, the scattered beam $\mathbf{I}_s$, and the scattering vector $\mathbf{q}$. Applying the standard equations for low-angle scattering from a dilute polymer solution,[35] the weight-average molecular weight M_w, the z average of the mean-square radius of gyration $\langle R_g^2\rangle_z$, and the second virial coefficient A_2 are determined through the formula

$$\frac{K_c}{R_\theta} = \frac{1}{M_w P(\theta)} + 2A_2 c \tag{1}$$

where K, the optical constant for vertically polarized incident light, is nominally provided through an equation deduced by Debye[37] for a solution containing isotropic scattering centers of refractive index comparable to the solvent's:

$$K = \frac{4\pi^2 n_0^2 (dn/dc)^2}{N_A \lambda^4} \tag{2}$$

The Rayleigh ratio, the polymer concentration, the solvent refractive index, the refractive index increment, Avogadro's number, and the wavelength of light in vacuum are represented as R_θ, c, n_0, (dn/dc), N_A, and λ, respectively. The inverse of the structure factor $P^{-1}(\theta)$ attains a universal form at sufficiently small $\mathbf{q}$:

$$P^{-1}(\theta) = \left[1 + \frac{16\pi^2 n_0^2 \langle R_g^2\rangle_z \sin^2(\theta/2)}{3\lambda^2}\right] \tag{3}$$

The range of $\mathbf{q}$ over which eq 3 is obeyed depends strongly on the actual conformation of the polymer chain. In the limit of zero angle and infinite dilution, the left side of eq 1 yields the reciprocal of the molecular weight, as $P(\theta)$ become unity at zero scattering angle θ. Experimentally, the Rayleigh ratio for a solution can be obtained

$$R_\theta = \frac{(I_\theta)_{\text{solution}}}{(I_{90})_{\text{toluene}}} R_{\theta,\text{toluene}} \tag{4}$$

where $(I_\theta)_{\text{solution}}$ represents the solution's scattered intensity (corrected for solvent scattering by subtraction), and $(I_{90})_{\text{toluene}}$ is the reference scattered intensity from toluene at 90°. The angle-independent value of $R_{\theta,\text{toluene}}$ is 14.1×10^{-6} cm^{-1}.[34] For poly(styrene) in toluene, dn/dc at $\lambda = 632.8$ nm is 0.11.[36]

During flow experiments the opposed jets are inserted so that their axis is perpendicular to the incident beam and in the horizontal plane. Superimposed on the sketch in Figure 2 is the principal axis $\mathbf{P}$ of molecular elongation at the stagnation point; this axis aligns with the orientation of the jets. In this geometry an extrapolation to $\theta = 0°$ simultaneously extrapolates the scattering vector $\mathbf{q}$ onto $\mathbf{P}$, enabling the radius of gyration parallel to the stretching direction, $R_{g,\parallel}$, to be evaluated. Thus, the normal low-angle-scattering extrapolation serves an additional purpose here, ensuring that the stretched dimension of the molecule is the one measured.

The preceding derivation may be inappropriate for a flow-oriented system. In particular, while eq 2 describes macromolecules containing isotropic scattering centers, most macromolecules contain optically anisotropic repeat units. This anisotropy, for example, is manifested in flow birefringence and depolarized scattering. The correction to standard scattering theory for an unoriented chain containing optically anisotropic chain structure has been shown to be small, at least when the chain is long and flexible. As discussed later, in a flow environment larger corrections appear necessary.

Flow Device. A uniaxial elongational flow field is created by using the opposed nozzle configuration pioneered by Keller and Odell.[1] Flow into two collinear and closely spaced glass capillaries is induced by the regulated and damped suction of a vacuum pump. The capillary diameters are 700 μm (i.d.), while the gap between the nozzle openings ranges from 0.3 to 1.0 mm. With a fluid of low viscosity, this device can generate elongation rates ranging from 100 to ~20 000 s^{-1}; at even higher elongation rates cavitation becomes a problem and the flow between the jets fluctuates. The elongation rate $\dot{\epsilon}$ is obtained by applying an approximate macroscopic balance across the gap[19]

$$\dot{\epsilon} = Q/\pi r^2 d \tag{5}$$

where Q is the total flow rate through the two nozzles, r is the radius of the nozzles, and d is the gap width. As described earlier, precise placement of the opposed nozzles in the light-scattering apparatus is critical. Thus far, scattering measurements have been performed only at the stagnation point, with a position error less than 50 μm; application of eq 5 therefore appears reasonable and consistent with previous literature.

When the flow device is in place, scattering measurements are only possible to $\theta = 60°$ (at the standard gap width $d = 1.0$ mm); larger scattering angles are occluded by the jets. The usable q range [where $q = (4\pi n_0/\lambda)\sin(\theta/2)$] is therefore 0.005 nm^{-1} < q < 0.015 nm^{-1}. The presence of the glass capillaries near the scattering volume contributes a small extraneous scattering contribution, although glass was purposely chosen to reduce this contribution by minimizing refractive index mismatches ($n_{\text{toluene}} = 1.4961$; $n_{\text{glass}} = 1.486$). Unwanted scattering is further reduced by polishing the capillary openings and performing background corrections with the jets in place. Solvent scattering has been verified to be independent of the flow rate through the jets; such independence is expected during laminar flow of an incompressible solvent because the local density fluctuations that give rise to solvent scattering remain uncoupled from flow fields at realizable strain rates.

Material. A monodisperse poly(styrene) standard of nominal molecular weight 20×10^6 (Polysciences; $M_w/M_n = 1.2$) is dissolved in spectroscopic grade toluene previously dedusted with 0.2- and 0.5-μm filters. Dilute solutions of concentrations from 3.75×10^{-5} to 1.14×10^{-4} g/mL are allowed to equilibrate with gentle stirring at room temperature for 2–3 days. These solutions are then filtered through 0.5-μm filters directly into the scattering vat. Intensity measurements at each angle require ~30 s, with a corresponding fluid loss from the vat of the order of 50–100 mL, depending on Q. Large volumes of solution must be available to keep the fluid level in the vat well above the scattering plane. During a single angular intensity scan, fluid is filtered into the vat at most five times. All solutions are discarded after being recycled eight times, a cycle consisting of filtering and elongational flow steps; under the most severe conditions, a 5% decrease in the M_w is observed at this point.

All concentrations are well below the overlap concentration c^* to avoid the complicated entanglement effects of the type reported by Chow et al.[24] for a similar flow environment. The highest concentration for the 20×10^6 MW poly(styrene) is approximately $0.1c^*$, where c^* is estimated from the reciprocal of the intrinsic viscosity. Polymer chains in flow can interact more strongly at low concentrations than in quiescent solution so c^*, defined in the normal way, is a poor indicator of the upper boundary of dilute behavior. Absence of intermolecular entanglement effects in the present experiment has been verified by birefringence observations, in which a steady, localized birefringent line is seen between the opposed nozzles under all flow conditions examined. Chow et al. demonstrated that the onset of entanglements correlates with the onset of unsteadiness in flow birefringence. Additional evidence against entanglement effects is the absence of distortion in the Zimm plot extrapolations to zero angle; strong curvature in these extrapolations is often used to demonstrate chain–chain interaction.

Results

Birefringence. Figure 3 displays the normalized birefringence intensity (retardance) as a function of $\dot{\epsilon}$ for a 100 ppm solution of 20×10^6 MW poly(styrene) in toluene. The curve follows the trends noted previously by Keller and Odell,[1] as well as those reported by Cathey and Fuller:[27] the birefringence intensity abruptly rises and saturates as $\dot{\epsilon}$ exceeds a threshold value. The strain rate at the onset of the birefringence upturn is ~900 s^{-1}, yielding a chain relaxation time of 1.1 ± 0.2 ms. This time quantitatively matches the theoretical Zimm relaxation time calculated

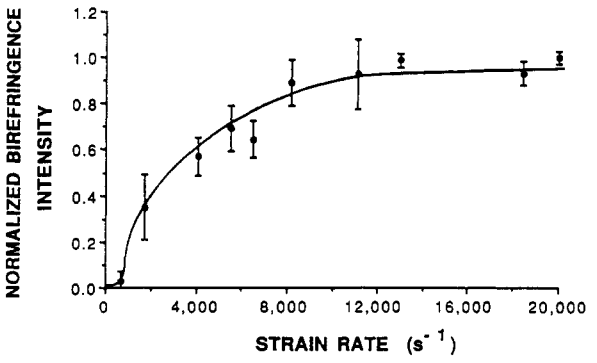

Figure 3. Normalized birefringence intensity as a function of strain rate $\dot{\epsilon}$ for a 100 ppm solution of 20×10^6 MW poly(styrene) in toluene.

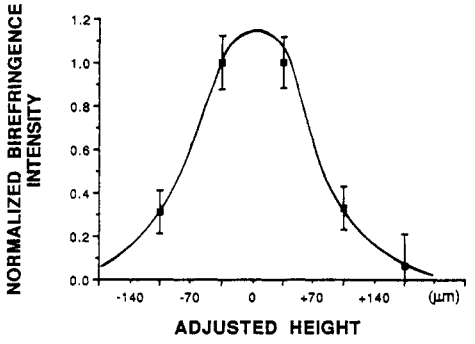

Figure 4. Birefringence intensity for a 100 ppm solution of 20×10^6 MW poly(styrene) in toluene as the flow device is adjusted vertically by small increments. A strain rate of 6500 s^{-1} is imposed simultaneously.

from the formula[17,38]

$$\tau_{Zimm} = 6.22\phi_0 R_{go}{}^3 \eta_s / RT \qquad (6)$$

where ϕ_0 is the Fox–Flory parameter (2.84×10^{23}), R_{go} is the unperturbed radius of gyration of poly(styrene) at room temperature (140 nm[36]), and η_s is the viscosity of toluene (0.58 cP). This close correspondence between the birefringence-determined characteristic time and the Zimm relaxation time is surprising since toluene is a good solvent for poly(styrene). Similar agreements have been noted during earlier experimental studies with good solvent systems,[1,27] and a theoretical explanation for the trend has been offered by Rabin.[39] Eventually, as $\dot{\epsilon}$ increases, the birefringence saturates and segmental orientation no longer changes with $\dot{\epsilon}$.

Observed through crossed polarizers, the birefringent region appears as a localized white line spanning the region between the two nozzles. This line lies on the axis of symmetry, possesses nearly constant width, and extends into the nozzle orifices. Figure 4 displays the birefringence intensity of the line as the entire flow assembly is moved vertically in small increments, holding the beam location and $\dot{\epsilon}$ fixed (6500 s^{-1}). The line width at half-height is 150 μm, a value somewhat greater than the characteristic dimension probed in subsequent scattering measurements. Taking into consideration the focused beam diameter ($1/e^2$ intensity contour diameter $\sim$140 μm) and the uncertainty in the vertical positioning of the jets, the spatial resolution of the birefringence scan is estimated at 50–75 μm, about half the line width. Some fraction of the width is thus attributable to the measurement method and not the true birefringence intensity distribution (convoluted by the cylindrical geometry). Cathey and Fuller[27] discussed how the width of the birefringent line in a similar opposed jets device varied with

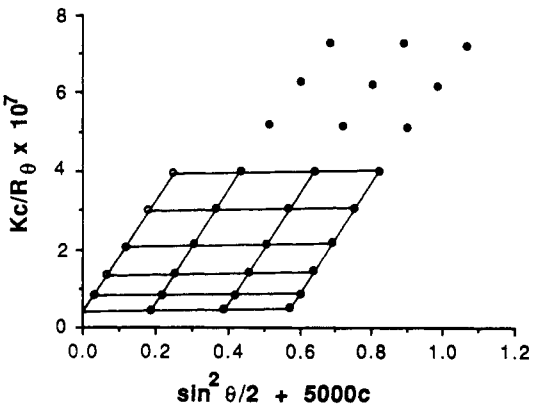

Figure 5. Zimm plot of the 20×10^6 MW sample in toluene. $c_1 = 3.74 \times 10^{-5}$ g/mL; $c_2 = 7.80 \times 10^{-5}$ g/mL; $c_3 = 1.142 \times 10^{-4}$ g/mL.

$\dot{\epsilon}$; in a good solvent [poly(styrene) in tricresyl phosphate at 25 °C] the width variation was found negligible within experimental error.

Light Scattering. Before specific scattering results are presented, a more detailed discussion of the size and shape of the scattering volume is merited. Analysis of the optical arrangement shows that the scattering volume can be imagined as a domain formed by the intersection of two cylinders, one associated with the incident beam and the other with the detection optics. As θ is decreased, the scattering volume is stretched along the incident beam by a factor $1/\sin\theta$, and the scattering volume develops a complex shape that is difficult to quantify. The incident beam intensity profile is also highly nonuniform, further complicating a direct calculation of the size of the scattering volume. This size, however, can be determined experimentally with data for the scattered intensity of an isotropic solvent

$$V = J_\theta / I_o R_\theta \qquad (7)$$

where I_o is the intensity per cross-sectional area of the incident beam at the scattering volume V, and J_θ is the scattered intensity per solid angle. Applying this method with toluene, the scattering volume is found to obey $V = (50\ \mu m)^3/\sin\theta$. The importance of this relationship is that it both confirms the optical design and places the scattering volume inside the birefringent line region at all θ; at the lowest measurement angle the projected length of the scattering volume along the incident beam is estimated at 140 μm, approximately matching the width at half-height of the birefringent region.

A Zimm plot for the 20×10^6 MW poly(styrene) standard dissolved in toluene is illustrated in Figure 5; no flow was imposed during data collection. Tracing a line of constant concentration, the curvature noted at angles above 60° reflects small contributions from molecular weight polydispersity and from nonlinearity in the single-chain structure factor $P(\theta)$. Therefore, to obtain M_w, R_g, and A_2, low-angle data analysis is applied only to intensity measurements at angles below 60°. The M_w, $\langle R_g^2\rangle_z^{1/2}$, and A_2 obtained via regressions over the linear portion of the plot are 23.4×10^6 g/mol, 345 nm, and 8.1×10^{-5} cm^3 mol/g^2, respectively. The measured $\langle R_g^2\rangle_z^{1/2}$ and A_2 compare well to literature values at this molecular weight, although employing such low concentrations limits the accuracy of the A_2 determination. Both the absolute precision and the reproducibility in the $\langle R_g^2\rangle_z^{1/2}$ measurement are estimated to be ±5%. Due to the necessary dual extrapolation of θ and c to zero, the experimental error in M_w is slightly larger (±10%).

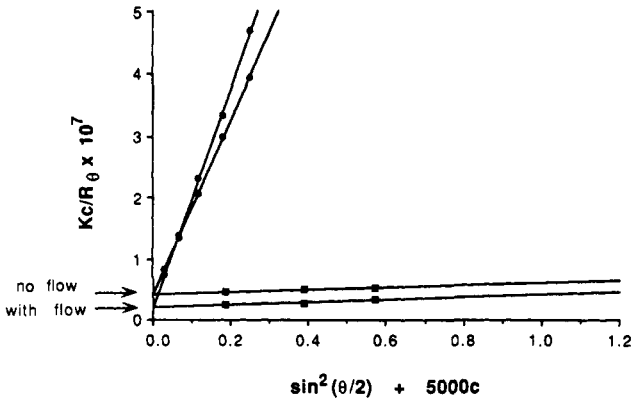

Figure 6. Zero angle (boxes) and zero concentration (circles) extrapolations from Zimm plots for poly(styrene) in toluene both with ($\dot{\epsilon}$ = 6500 s^{-1}) and without flow. The optical constant K has been estimated from the refractive index increment. Darkened symbols are with flow and open symbols are without flow.

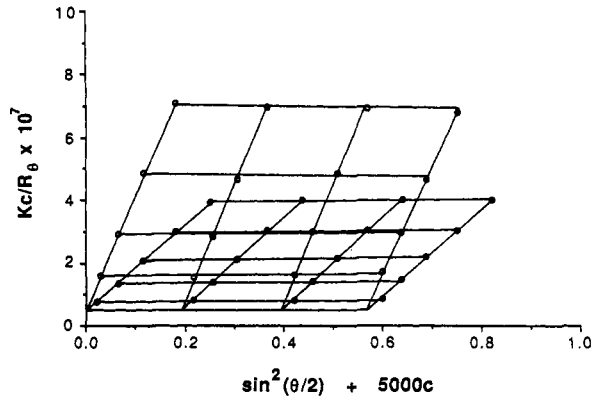

Figure 7. Superposition of Zimm plots with ($\dot{\epsilon}$ = 6500 s^{-1}) and without flow. The optical constant K in the presence of flow has been adjusted to provide the same y intercept as in the absence of flow.

As the polymer chains stretch in the flow field, the scattered intensity at all θ is expected to decrease compared to the quiescent state; such a trend will simply reflect an increased molecular dimension projected onto the direction of the scattering vector. Contrary to expectation, however, the intensity decreases only at high angles ($30° < \theta < 60°$). At low angles the scattered intensity actually increases compared to the quiescent state. Consequently, there is a shift in the Zimm plot y intercept, suggesting an implausible increase in M_w. Figure 6 displays the nominal Zimm plot intercept alongside the extrapolated $c = 0$ and $\theta = 0$ lines employed in obtaining the intercept value. The implausible increase in M_w with flow is well outside the range of experimental error. One also notes that the (apparent) A_2 has not changed under flow.

The intercept shift is attributed to the optical anisotropy of the flow-oriented solution. The birefringence of flowing poly(styrene) is negative; in other words, pendent phenyl groups produce excess polarizability in the direction perpendicular to the chain backbone. As a poly(styrene) chain becomes stretched between the opposed jets, an increasing fraction of its segments are oriented, from a statistical standpoint, in the flow direction; this orientation is associated with the perpendicular alignment of phenyl groups. With the incident beam vertically polarized, an increase in scattered intensity will be observed in the horizontal plane, shifting downward the reciprocal intensity data of a Zimm plot. The experiments point toward a single-chain basis for this optical anisotropy effect, inasmuch as Zimm plot lines corresponding to constant polymer concentration exhibit the same slope across the entire concentration range examined. These slopes would vary with concentration if entanglements played any role in the mechanism of segmental orientation.

A conventional assumption is that the refractive index increment is a measure of the excess polarizability of a polymer solution. The optical constant K of eq 2 actually becomes a tensorial quantity in a flow-deformed solution, and additional information is needed to isolate the perpendicular component. An empirical fix is simple: knowing that chain scission has been carefully avoided, the y intercept of the Zimm plot is adjusted to its appropriate no flow value through a multiplicative correction to the optical constant K. The ratio of the intercept in the case of no flow to that in the presence of flow ranges from 1.5 to 2.7, increasing, and then saturating with $\dot{\epsilon}$.

We have developed a theoretical analysis to substantiate the polarizability correction. In this approach the ratio of zero-angle-scattered intensity for randomly oriented poly(styrene) segments (I_{NF}) to that for fully aligned segments (I_F) is directly calculated from molecular considerations. Components of the polarizability tensor are determined from the bond polarizabilities of the repeat unit.[40] The calculated value of the ratio I_{NF}/I_F ranges from 1.1 to 1.3, depending on assumptions about tacticity and the local conformational states of the stretched chain. As seen before, the empirically derived correction ratios are substantially larger, exceeding any uncertainty in the theoretical analysis. One possible explanation for the discrepancy is that solvent orientation may contribute to solution optical anisotropy. Alignment of toluene molecules in layers surrounding the deformed poly(styrene) chain could increase the perpendicular polarizability. This trend should not be surprising in light of the many birefringence studies of polymer solutions and gels that have found strongly solvent dependent segmental optical anisotropies.[28,29] Short-range orientational order of anisotropic solvent molecules can give rise to abnormally large optical anisotropies.[41] We have no independent experimental data for the optical anisotropy tensor for the poly(styrene)/toluene system employed in this study. Such data might be provided by quantitative birefringence or depolarized scattering measurements.

Figure 7 is a Zimm plot for $\dot{\epsilon} = 6500\ s^{-1}$, with the empirical correction applied to the optical constant K. Superimposed is the scattering data for the same solution in the absence of flow. An increase in the radius of gyration in the stretching direction is clear. The low-angle-scattering approximation required in analyzing these types of data will eventually become inapplicable as the chain undergoes more substantial stretching, i.e., when $qR_{g,\parallel}$ is too large. Higher order terms of $P^{-1}(\theta)$ will then create curvature of the extrapolated $c = 0$ line in the Zimm plot. No substantial curvature, however, has yet been observed for Zimm plots under flow, at least for θ less than 60°. In the flow under discussion, the dimensionless scattering range $qR_{g,\parallel}$ varies from 2.5 to 6.

The range over which low-angle-scattering theory can be employed to interpret intensity information is strongly dependent on molecular structure. Unfortunately, in the absence of any confirmed theory for the structure factor in flow, the linear proportionality of the $P^{-1}(\theta)$ with the square of $qR_{g,\parallel}$ is the only test for the low-angle analysis. Although the cited $qR_{g,\parallel}$ range seems rather large, it is significant to note that the Debye function for monodisperse Gaussian chains remains closely linear to ranges well beyond those studied here; for example, arbitrarily assuming that the Debye function is correct for the scattering data at 6500 s^{-1}, the error in $R_{g,\parallel}$ from linearization is

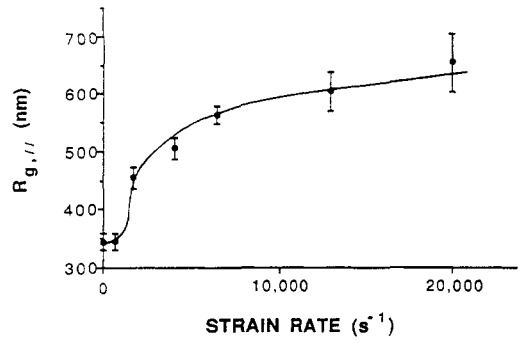

Figure 8. Change in $R_{g,\parallel}$ as the elongation rate is varied. The data can be compared to those in Figure 3, which displays the flow birefringence response under identical conditions.

~10%. Uncertainty at such levels is not important to the conclusions of this study. It is also noted that the reported equilibrium (i.e., no flow) radius of gyration, $R_{g,eq}$, of 20 × 10^6 MW poly(styrene) in toluene, calculated here over the range $1.7 < qR_g < 4.5$, nearly matches the accepted literature value. In this case, as with flow, the $c = 0$ extrapolation is linear, indicating that structure-dependent corrections are only important at larger angles than employed here. A significant effort was made to conduct scattering at still lower angles, but the experimental obstacles in the present apparatus appear overwhelming.

The extrapolation of **q** to the direction of molecular stretching **P** as the scattering angle θ is rotated to 0° produces an additional error that is sensitive to the details of the structure factor. For a molecule strongly deformed in the flow direction, the apparent molecular dimension will increase as θ is reduced. The result is a $c = 0$ extrapolation on the Zimm plot that is concave downward; such data have not been observed. To further ensure that such complications are unimportant, a few experiments were conducted so that **q** always pointed along **P**. This superposition was accomplished by manually rotating the flow device as θ was varied; alignments problems were severe. The Zimm plots so generated were identical with those reported here. Future versions of the scattering apparatus will incorporate an additional rotational stage so that this alignment condition is always obeyed.

Chain stretching as a function of $\dot{\epsilon}$ for the 20 × 10^6 MW sample is shown in Figure 8; this curve is the key result of the present study. Deformation begins at the same strain rate as the birefringence-determined segmental alignment, correlating with the inverse of the Zimm relaxation time. At $\dot{\epsilon}$ below the onset, no indication of chain deformation is observed, a result again consistent with prior birefringence studies. Above $\dot{\epsilon}_{crit}$, or equivalently above De_{crit}, the stretched chain's dimension rises abruptly over a span of $\dot{\epsilon}$ that is substantially less than 1 order of magnitude. Finally, the chain deformation appears to attain a plateau, with little additional stretching as $\dot{\epsilon}$ increases. The largest observed extension ratio, defined as $R_{g,\parallel}/R_{g,eq}$, is of the order 2, even when De_{crit} is exceeded by a factor of 10. Thus, the data do not support a picture of total chain unraveling in the opposed jets flow device at high $\dot{\epsilon}$, even though the relative birefringence has saturated. The error bars on the data points of Figure 8 reflect ±1 standard deviation, determined by a statistical analysis of the scattering data; there is no appreciable increase in this error level with flow. In fact, the rapid motion of the fluid through the jets reduces problems associated with dust scattering. Without the polarizability correction discussed earlier, the general shape of the curve in Figure 8 would be much the same, except that the plateau at high $\dot{\epsilon}$ would be lowered by a factor of ~50%.

Surprisingly, the onset and plateau of the stretching curve in Figure 8 appear to correlate with the flow birefringence data for the same solution (Figure 3). After appropriate normalization, Figure 8 and Figure 3 superimpose within the experimental error in the two data sets; the physical significance of this overlap is not clear.

Discussion

The rather low extension ratios experimentally observed must, in some way, be ascribed to the limited residence times of polymer chains in the vicinity of a stagnation point. A flexible polymer subject to transient elongational flow has only a finite time to unravel and extend before leaving the region of highest elongation rate. If the chain could remain forever, the stretched conformation would be overwhelmingly preferred at high De. Saturation of the birefringence intensity indicates that orientation at the segmental level is more rapidly attained than total chain unraveling. Some of the simulations reported in the literature, for example, those of Acierno et al.[12] and of Liu,[15] support this picture of a time-dependent response to flow, as do the elongational viscosity data of Cathey and Fuller[27] in θ solvents. It is noted, however, that the excluded volume of the chain, including uncrossability, has never been incorporated into the simulations, and these additional constraints could play a significant role in further slowing global deformation while leaving segmental orientation quite facile.

The chain-halving result for flow-induced degradation of flexible polymers in the opposed jets device has often been cited as convincing evidence for chain unraveling.[1] Midpoint cleavage is not perfect, however, and it remains unclear how to reconcile degradation results in transient flow, also displaying chain halving,[42] with a picture of complete uncoiling. In some of the transient flows reported in the literature even an affine deformation of the coil with the surrounding fluid would leave the coils far from an extended conformation. The scattering results can also be placed in accord with the degradation work by considering the chain population that each technique probes. It is not certain that chains break at spatial locations throughout the birefringent line. The chain size reported here is an average across a region of approximately the diameter of this line and centered at the stagnation point; chains may degrade in a much more restricted volume centered very close to the stagnation point or at some other position outside our scattering volume.

To test some of these ideas, the scattering volume has been reduced by focusing the incident beam to a waist 3× smaller than for the experiments so far reported; except for a significant reduction in scattered intensity, no effect was noted at $\dot{\epsilon} = 6500\ s^{-1}$. Low-angle scattering measures the mean-square radius of gyration so the bias of the method is toward the most deformed molecules. These two considerations suggest that the most deformed molecules are sampled in the scattering experiment and that molecular deformation is indeed not so great. This result is essentially the one reported by Smith et al.[30] many years ago. Future contributions will discuss experiments at additional molecular weights and in different solvents.

Acknowledgment. This work was supported by NSF Grant DMR-8618534. We thank Professors K. Langley and M. Muthukumar for many helpful discussions and suggestions.

References and Notes

(1) Keller, A.; Odell, J. A. *Colloid Polymer Sci.* **1985**, *263*, 181.

(2) Farrell, C. J.; Keller, A.; Miles, M. J.; Pope, D. P. *Polymer* **1980**, *21*, 1292.
(3) Peterlin, A. *Makromol. Chem.* **1961**, *44–46*, 338.
(4) de Gennes, P. G. *J. Chem. Phys.* **1974**, *60*, 5030.
(5) Hinch, E. *J. Phys. Fluids* **1972**, *20*, s22.
(6) Fuller, E. J.; Leal, L. G. *J. Non-Newtonian Fluid Mech.* **1981**, *8*, 271.
(7) Fan, X. J.; Bird, R. B. Rheology Research Center Report 96, University of Wisconsin—Madison, 1984.
(8) Ottinger, H. C. *J. Chem. Phys.* **1987**, *86*, 3731.
(9) Larson, R. G.; Magda, J. J. *Macromolecules* **1989**, *22*, 3004.
(10) Rabin, Y. *J. Chem. Phys.* **1988**, *88*, 4014.
(11) Weist, J. M.; Bird, R. B. *Rheology* Research Center Report 116, University of Wisconsin—Madison, 1988.
(12) Acierno, D.; Titomanlio, G.; Marrucci, G. *J. Polym. Sci., Polym. Phys. Ed.* **1974**, *12*, 2177.
(13) Rallison, J. M.; Hinch, E. J. *J. Non-Newtonian Fluid Mech.* **1988**, *29*, 37.
(14) Ryskin, G. *Phys. Rev. Lett.* **1987**, *59*, 2059.
(15) Liu, T. W. *J. Chem. Phys.* **1989**, *90*, 5826.
(16) Rouse, P. E. *J. Chem. Phys.* **1953**, *21*, 1272.
(17) Zimm, B. H. *J. Chem. Phys.* **1956**, *24*, 269.
(18) Kramers, H. A. *Physica* **1944**, *11*, 1.
(19) Fuller, G. G.; Cathey, C. A.; Hubbard, B.; Zebrowski, B. E. *J. Rheol.* **1987**, *31*, 235.
(20) Peiffer, D. G.; Kim, M. W.; Lundberg, R. D. *Polymer* **1986**, *27*, 493.
(21) Mackley, M. R.; Keller, A. *Philos. Trans. R. Soc. London* **1975**, *278*, 29.
(22) Pope, D. P.; Keller, A. *Colloid Polym. Sci.* **1978**, *256*, 751.
(23) Peiffer, D. G.; Kim, M. W.; Schulz, D. N. *J. Polym. Sci., Polym. Phys. Ed.* **1987**, *25*, 1615.
(24) Chow, A.; Keller, A.; Muller, A. J.; Odell, J. A. *Macromolecules* **1988**, *21*, 250.
(25) Odell, J. A.; Muller, A. J.; Keller, A. *Polymer* **1988**, *29*, 1179.
(26) Brestkin, Y. V.; Saddikov, I. S.; Agranova, S. A.; Baranov, V. G.; Frenkel, S. *Polym. Bull.* **1986**, *15*, 147.
(27) Cathey, C. A.; Fuller, G. G. *J. Non-Newtonian Fluid Mech.* **1990**, *34*, 63.
(28) Janaschitz-Kriegl, H. *Adv. Polym. Sci.* **1969**, *6*, 170.
(29) Frisman, E. V.; Dadivanian, A. K. *J. Polym. Sci., Part C* **1967**, *16*, 1001.
(30) Smith, K. A.; Merrill, E. W.; Peebles, L. H.; Banijamali, S. H. *Colloq. Int. C.N.R.S.* **1975**, *No. 233*, 341.
(31) Lumley, J. L. *Phys. Fluids* **1977**, *20*, s64.
(32) Armstrong, R. C.; Gupta, S. K.; Basaran, O. *Polym. Eng. Sci.* **1980**, *20*, 469.
(33) Chu, B. *Laser Light Scattering*; Academic Press: New York, 1974.
(34) Haller, H. R.; Destor, C.; Cannell, D. S. *Rev. Sci. Instrum.* **1983**, *54*, 973.
(35) Yamakawa, H. *Modern Theory of Polymer Solutions*; Harper & Row: New York, 1971.
(36) Brandrup, J.; Immergut, E. H. *Polymer Handbook*, 3rd ed.; John Wiley & Sons: New York, 1989.
(37) Debye, P. *J. Phys. Colloid Chem.* **1947**, *51*, 18.
(38) Zimm, B. H.; Roe, G. M.; Epstein, L. F. *J. Chem. Phys.* **1956**, *24*, 279.
(39) Rabin, Y.; Henyey, F. S.; Pathria, R. K. *Phys. Rev. Lett.* **1985**, *55*, 201.
(40) Stein, R. S. *J. Appl. Phys.* **1961**, *32*, 1280.
(41) Gent, A. N. *Macromolecules* **1969**, *2*, 262.
(42) Nguyen, T. Q.; Kausch, H. H. *J. Non-Newtonian Fluid Mech.* **1988**, *30*, 125.